Determination of resist parameters using the extended Nijboer-Zernike theory

Peter Dirksen[a], Joseph Braat[b], Augustus J.E.M. Janssen[c], Ad Leeuwestein[c]
Hans Kwinten[a] and David Van Steenwinckel[a]

[a]Philips Research Leuven, Belgium
[b]Delft University of Technology, The Netherlands
[c]Philips Research Laboratories, The Netherlands

ABSTRACT

This study presents an experimental method to determine the resist parameters that are at the origin of a general blurring of the projected aerial image. The resist model includes the effects of diffusion in the horizontal plane and a second cause for image blur that originates from a stochastic variation of the focus parameter. The used mathematical framework is the so-called Extended Nijboer-Zernike (ENZ) theory. The experimental procedure to extract the model parameters is demonstrated for several 193 nm resists under various conditions of post exposure baking temperature and baking time. The advantage of our approach is a clear separation between the optical parameters, such as feature size, projection lens aberrations and the illuminator setting on the one hand and process parameters introducing blur on the other.

Keywords: Optical lithography, resist, diffusion constant, focus noise, point-spread function, Extended Nijboer-Zernike theory.

1. INTRODUCTION

Nowadays, optical lithography is able to print sub-40 nm lines using a binary mask and advanced resist processing.[1] The line width is of the same order of magnitude as the image blur caused by the effects of acid diffusion. In addition the depth of focus, about 300 nm, is of the same order of magnitude as the stochastic variation of the focus parameter. An extended diffused aerial image model is a simple, but powerful method to take these image blur effects into account.

The influence of longitudinal and transverse vibrations on the transfer function is described in reference.[2] It was shown that both vibrations have a degrading effect on the image quality. For a step and scan system the effects of image blur in the horizontal plane are described in references.[3–5] Here, image blur originates from mechanical noise and synchronization errors. A probability density function was used to describe the statistics of the disturbance. Mathematically, a convolution of the probability density function with the static aerial image is used to calculate a diffused aerial image. The application of a diffused aerial image to optical proximity corrections is described in ref,[6] where a Gaussian probability density function is used to describe the effects of acid diffusion during the post exposure baking process. In various publications the validity of the Diffused Aerial Image Model (DAIM) was assessed.[7,8] It was concluded that DAIM is a good predictor not only for lines and spaces but also for 2D structures such as contact holes. The accuracy of DAIM was found to be comparable to full resist models.

In this study we describe an extension of the DAIM model. Not only do we include the effects of diffusion in the horizontal plane but also a second cause for image blur that originates from a stochastic variation of the focus parameter. Therefore, both the radial coordinate r and focal coordinate f are treated as a stochastic

Further author information: (Send correspondence to peter.dirksen@philips.com)
P.D., H.K. and D.V.S., Philips Research Leuven, Kapeldreef 75, B-3001 Leuven, Belgium
J.B.: Optics Research Group, Department of Applied Sciences, Delft University of Technology, Lorentzweg 1, NL-2628 CJ Delft, The Netherlands
A.J.E.M.J. and A.L.: Philips Research Laboratories, WO-02 and WY-51, NL-5656 AA Eindhoven, The Netherlands

parameter with a standard deviation σ_r and σ_f respectively. The two parameters describe the transition from aerial image to resist image; therefore, we call σ_r and σ_f the resist parameters of the extended diffused aerial image model.

In order to estimate the resist parameters, it is our first task to make a clear separation between optical parameters, such as feature size, projection lens aberrations and the illuminator setting on one hand and resist parameters on the other. For this purpose we use the Extended Nijboer-Zernike (ENZ) theory,[9–12] which is designed for computing the aberrated through-focus point-spread function. The used mathematical framework is presented and the experimental procedure to extract the resist parameters is demonstrated. The experimental procedure involves the analysis of a focus-exposure matrix of an isolated contact hole. The results of several Arf resists for various conditions of Post Exposure Baking (PEB) temperature and PEB time are shown. For our experiments we use a 193 nm wafer scanner.

The paper is organized as follows. Section 2 describes the used mathematical background of the point-spread function in the presence of diffusion in the horizontal plane and image blur that originates from a stochastic variation of the focus parameter. Section 3 describes the procedure to retrieve the resist parameters from a through-focus intensity point-spread function. The procedure is tested on numerical simulated diffused aerial images. Section 4 presents the experimental results obtained on several Arf resists under various conditions. The Appendix 6 presents the mathematical definitions of the normalizated coordinates and the $V_{n,m}$-radial functions. It is also indicated how the finite object size is incorporated in the ENZ-theory. In addition, we indicate how to calculate the convolution of a rotational symmetrical function in an efficient way.

2. MATHEMATICAL FRAMEWORK

There are several processes that cause blurring in the horizontal plane of the projected aerial image. The first process is wafer stage noise in the (X,Y) direction. In the exposed areas of a chemically amplified resist (CAR), acid is generated and diffuses during PEB.[13,14] In addition, a chemical base or quencher, also present in the resist, influences the final acid distribution. The development process[15] and the metrology tool also influences the shape of the final observed resist profile. In our model, the combined effect is described by a single diffusion parameter σ_r. A second cause for image blur originates from a stochastic variation of the focus parameter, caused by, for example, wafer stage noise in the Z-direction. In our model the effect is described by the focus noise parameter σ_f. For a step and scan system there are additional sources of image blur,[3] related to the scanning motion of the wafer and reticle stage such as synchronization errors. Also distortion and field curvature contribute to image blur, as the point-spread function is scanned through the field of the projection lens.

2.1. The influence of spherical aberration, diffusion and focus noise on the intensity point-spread function

Below we briefly review the Extended Nijboer-Zernike theory to calculate the intensity point-spread function and indicate how the effects of aberrations, diffusion and focus noise can be taken into account. Although the analysis can be generalized, for simplicity we restrict ourselves to low order spherical aberration and rotationally symmetrical blur functions.

The point-spread function or impulse response of an optical system is the image of an infinitely small object. In practice, an object having a diameter of the order of $\sim \frac{\lambda}{2NA}$ is a fair approximation. From a practical point of view, it is favourable to use a somewhat larger hole size on the reticle since the increased amount of transmitted light significantly reduces the exposure time, making the experiment more practical. The effect of a non-negligible hole size on the point-spread function is taken into account by the theory, as indicated in the appendix.

The calculation of the point-spread function of general aberrations $A \cdot \exp(i\phi)$, with possible non-constant transmission amplitude A is shown in ref.[12] In our restricted analysis, we assume rotationally symmetrical blur functions. Then it is sufficient to consider only the rotationally symmetrical terms of the intensity point-spread function. In addition we assume unit transmission $A = 1$.

The first blur effect is position noise. For mechanical Gaussian noise in the horizontal plane, without preferential direction, the 2-dimensional spectral density function reads:

$$d(x,y) = \frac{2}{\sigma_r^2} \exp\left(\frac{-(x^2+y^2)}{2\sigma_r^2}\right) . \tag{1}$$

The blurred image $I'(x,y,f)$ is obtained by a 2-dimensional convolution of the static image $I(x,y,f)$ and the spectral density function:

$$I'(x,y,f) = \int_{-\infty}^{+\infty} I(x',y',f) \cdot d(x-x',y-y')dx'dy' . \tag{2}$$

Examples of various other spectral density functions describing sinusoidal vibrations, distortion averaging and synchronization errors are described elsewhere.[3] The second image blur effect originates from acid diffusion during the post exposure baking process. Now the standard deviation is interpreted as the Fickian diffusion length

$$\sigma_r = \sqrt{2Dt} , \tag{3}$$

with D the acid diffusion coefficient and t the baking time. Under the condition of small and independent disturbances, a total RMS-noise amplitude can be defined, which is represented by the single parameter σ_r.

A third cause for image blur originates from a stochastic variation of the focus parameter. This effect can be taken into account by convolving the point-spread function in the focus variable f by a distribution function:

$$fn(f) = \frac{1}{\sigma_f\sqrt{2\pi}} \exp\left(\frac{-f^2}{2\sigma_f^2}\right) . \tag{4}$$

We assume that the function fn has a symmetrical distribution around its mean with standard deviation σ_f.

For a good lens, having small aberrations, the intensity point-spread function is written as a linear summation of basic functions. When low order spherical aberration is present, the point-spread function has an additional term proportional to the coefficient α_9 (we use the Fringe Zernike convention). It can be shown that for small values of (σ_R, σ_F), the intensity point-spread function has two additional contributions $D(r,f)$ and $F(r,f)$. In its simplest form, the intensity point-spread function is written as:

$$I(r,f) \approx |V_{0,0}(r,f)|^2 + \alpha_9 \cdot Re\{2iV_{0,0}^*(r,f)V_{4,0}(r,f)\} + \sigma_r^2 \cdot D(r,f) + \sigma_f^2 \cdot F(r,f) . \tag{5}$$

$D(r,f)$ and $F(r,f)$ represent the effect of diffusion and focus noise respectively, and are independent of (σ_r, σ_f). Thus, the effects of aberrations, diffusion and focus noise are additive. That means that the three effects, simply add to the ideal aberration-free point-spread function $|V_{0,0}(r,f)|^2$. Also note that the effects of diffusion and focus noise depend on the variance (σ_r, σ_f) in a quadratic way and that the effect of spherical aberration depends linearly on the coefficient α_9. The Appendix 6 gives the definitions of the scaled coordinates (r,f) as well as the definition of the radial functions $V_{n,m}(r,f)$. The radial functions $D(r,f)$ and $F(r,f)$ can be obtained by numerical integration:

$$D(r,f) = \lim_{\sigma_r \to 0} \left[\frac{|V_{0,0}(r,f)|^2 \otimes d(r) - |V_{0,0}(r,f)|^2}{\sigma_r^2}\right] , \; F(r,f) = \lim_{\sigma_f \to 0} \left[\frac{|V_{0,0}(r,f)|^2 \otimes fn(f) - |V_{0,0}(r,f)|^2}{\sigma_f^2}\right] . \tag{6}$$

The procedure essentially involves a numerical convolution algorithm using the functions in Eqns. (1) and (4) as convolution kernels, see the Appendix 6.4 for details. We note that spherical aberration has a direct impact on the point-spread function itself, whereas the diffusion and the focus noise manifest themselves as convolution operations performed on the intensity point-spread function.

Figure 1 shows contour plots of the intensity point-spread function $I(r,f)$, illustrating the influence of spherical aberration, diffusion and focus noise on an aberration-free intensity point-spread function for $\lambda = 193$ nm and $NA = 0.63$. The six contours represent lines of equal intensity in the range of [0.05, 0.1, 0.3, 0.5, 0.7, 0.9] of the maximum intensity. Figure 1, left-hand picture, illustrates the intensity point-spread function when a certain amount of spherical aberration is included. Figure 1, central picture, shows the diffused Airy pattern when a diffusion term with a certain variance σ_r is included. Figure 1, right-hand picture, shows the diffused Airy pattern when focus noise with a certain variance σ_f is included. The impact of spherical aberration, diffusion and focus noise on the point-spread function is seen to be quite different.

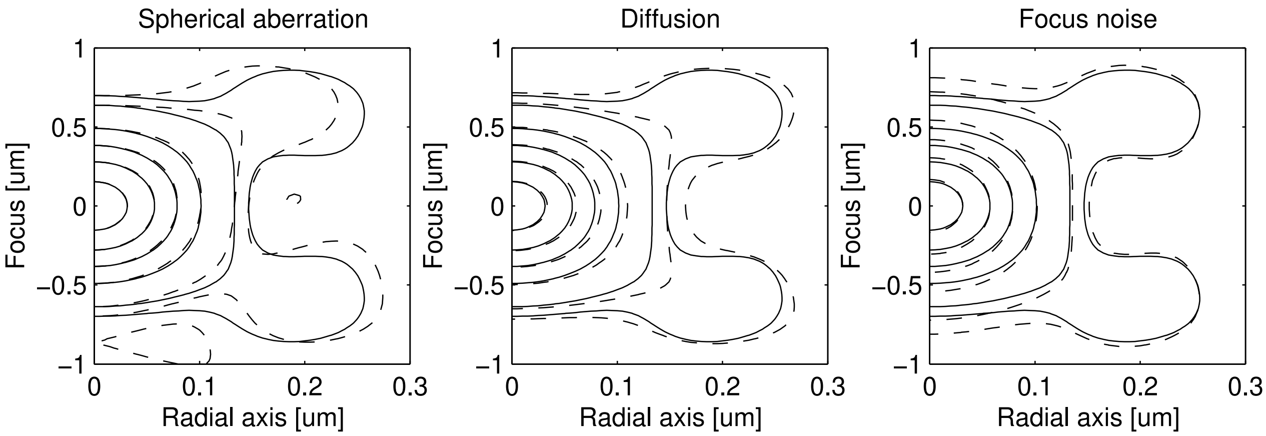

Figure 1. Contour plots of the intensity point-spread function $I(r, f)$ showing the influence of spherical aberration, diffusion and focus noise on an aberration-free intensity point-spread function (solid lines) for $\lambda = 193$ nm and $NA = 0.63$. The six contours are lines of equal intensity in the range from [0.9 0.7 0.5 0.3 0.1 0.05] of the maximum intensity. **Left**: with spherical aberration (dashed lines), **mid**: with diffusion (dashed lines) and **right**: with focus noise (dashed lines). Note that the influence of spherical, diffusion and focus noise are quite different.

3. RETRIEVING THE OPTICAL PARAMETERS AND RESIST PARAMETERS

The three effects, spherical aberration, diffusion and focus noise, behave in an orthogonal way and leave a unique finger print on the PSF. Spherical aberration causes a through-focus asymmetry, i.e. $I(r, f) \neq I(r, -f)$. Diffusion stretches the intensity point-spread function (PSF) in the (X,Y) plane and causes a broadening or loss of resolution of the PSF. On the other hand, focus noise stretches the PSF in the Z- direction, almost without broadening it in the (X,Y) direction. This effect is known as 'focus drilling' and causes an increase in depth of focus at the expense of exposure lattitude. Both diffusion and focus noise maintain the through-focus symmetry $I(r, f) = I(r, -f)$. As a result of their different impact, the three contributions to the intensity PSF can be separated experimentally.

Eq. (5) represents a near-identity between the measured quantity on the left and the theoretical quantity on the right. The procedure to retrieve the parameters is very similar to aberration retrieval, as described in reference.[12] By taking inner products with the various intensity functions involved in Eq. (5), the coefficients can be estimated on solving a linear system of equations. Note that this linear model is accurate for small parameter values only.

In order to validate the retrieval procedure, we retrieved the noise parameters from SOLID-C[16] calculated diffused aerial images. Position noise and focus noise are both implemented in the lithographic simulator SOLID-C in the options "detailed scanner noise in (X,Y,Z)". The simulator uses the same settings as the experiments: the exposure wavelength is $\lambda = 193$ nm and the numerical aperture is $NA = 0.63$. For the optical model we used the so-called high NA - scalar transfer matrix model, aberration-free case. Next, we used the ENZ-theory to retrieve the resist parameters from the simulated aerial image. In the table below we compare the SOLID-C input parameter with the retrieved parameters (σ_r, σ_f). The results shown in the table, are obtained by an extended analysis procedure that takes second order, non-linear effects into account.

Input SOLID-C		Retrieved by ENZ	
σ_r [nm]	σ_f [nm]	σ_r [nm]	σ_f [nm]
0	0	0	0
20	0	18	0
40	0	36	0
0	100	0	100
0	200	0	200
10	50	7	50
20	100	18	100
40	200	39	180

We observe a good agreement between input and retrieved parameters. The effects of diffusion and focus noise behave indeed independently. The small differences between input and retrieved parameters correspond to very small intensity differences, well below 1 %, of the maximum amplitude of the point-spread function.

4. EXPERIMENTAL DETERMINATION OF RESIST PARAMETERS

This section describes the basic experiment to determine the resist parameters. The reticle is a simple chrome on quartz reticle with a $4 \times 0.15 = 0.6\,\mu m$ transparent hole. An ASML PAS5500/950 system with a $\lambda = 193$ nm, $NA = 0.63$ projection lens is used to image the reticle onto resist on a *SiON* anti-reflective coating. Using *SiON* instead of an organic anti-reflective coating has the advantage that it provides a good contrast in the SEM. Next, we record a focus-exposure matrix of the isolated contact hole in photoresist and measure the hole diameter in a SEM. A Hitachi 9200 CD-SEM, under job control, collects all images. The data reduction is done off-line. A

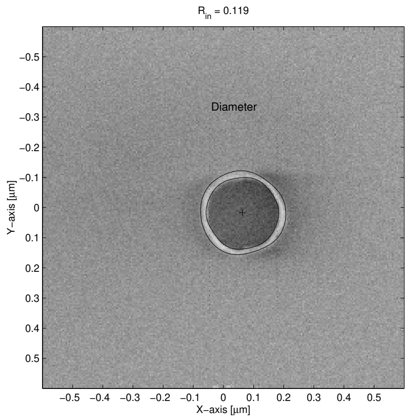

Figure 2: An example of a single pinhole exposure.

typical example of a SEM image is shown in figure 2, where we extract the inner diameter of the contact hole. These data are interpreted as the through-focus intensity point-spread function of the projection lens. Figure 3 shows an example of a focus-exposure matrix of the contact hole and the corresponding point-spread function. We observe a best match for the spherical aberration parameter $\alpha_9 = 34\,m\lambda$, the diffusion parameter $\sigma_r = 31$ nm and a focus noise parameter of $\sigma_f = 195$ nm. Figure 4 shows the resulting fit to the experimental data. The mean square relative error equals 1.9 %.

4.1. Experimental results for various resists under various conditions

Figure 5 left-hand picture, shows the dependence of the measured diffusion length σ_r on the post exposure baking temperature for two resists. The standard resist has a larger diffusion parameter and steeper temperature dependence compared to the low-PEB- sensitive resist. The increase of σ_r reflects the expected increase of acid

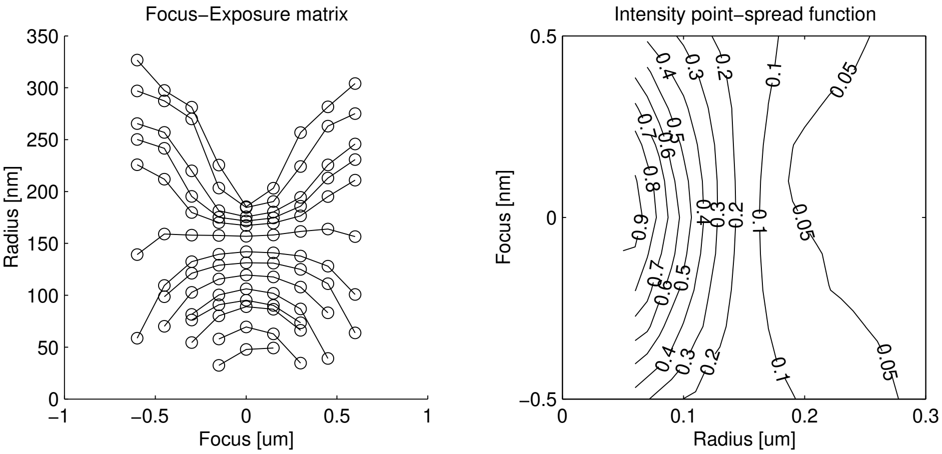

Figure 3. Left: *Focus-exposure matrix of an isolated contact hole. The radius of the developed resist contour as a function of the focus setting; the parameter yielding the set of curves is the exposure dose, ranging from 20 to* $800mJ/cm^2$. **Right**: *A contour plot of the intensity point-spread function of the projection lens, in a cross-section containing the vertical axis. The data of the focus-exposure matrix is used.*

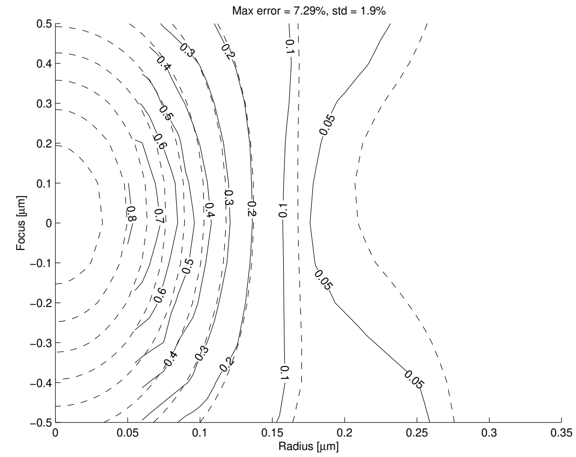

Figure 4. *Contour plot of the experimental intensity point-spread function (solid lines) compared to the data fit (dashed lines) for low- PEB-sensitive resist (at 130 degree PEB temperature). We observe a best match for the spherical aberration parameter* $\alpha_9 = 34m\lambda$*, the diffusion parameter* $\sigma_r = 31$ *nm and a focus noise of* $\sigma_f = 195$ *nm.*

diffusion length versus baking temperature. Figure 5 right-hand picture, shows PEB time dependence for the standard resist. The solid curve is a fit to the experimental data, assuming an *Offset* + $\sqrt(2D \cdot t)$ increase of the diffusion parameter with time, see Eq. (3). The mean square error of the experimental data with respect to the fitted curve is 1.6 nm.

Figure 6 summarizes our results of diffusion and focus noise measurements. The diffusion parameter measurements of different resits are summarized in figure 6 left-hand picture. We have included the results of contact hole resist (A), a low PEB-sensitive resist (B), our 'standard' resist (C) and also the result for a 157 nm resist (E) that has been exposed on the 193 scanner. This result indicates that our method applicable to various resist types and chemistries. The contact hole resist has clearly the smallest diffusion length. In an additional experiment, the resist vendor has modified the standard resist on request and replaced the PAG anion by a smaller one. The modified resist is indicated as resist (D). This resulted in a release of smaller acid molecules

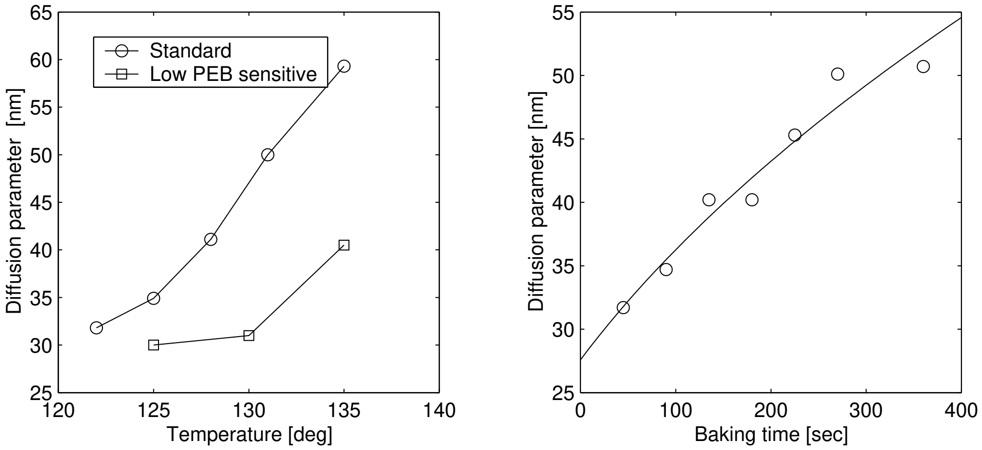

Figure 5. Left: The dependence of the diffusion parameter σ_r on the post exposure bake temperature. The solid lines serve as a visual guideline. **Right**: The dependence of the diffusion parameter σ_r on the baking time of the PEB. Here, the solid line represents the *Offset* $+ \sqrt{2D \cdot t}$ dependence. Both measurements reflect the expected increase of acid diffusion of a chemically amplified resist with PEB time and temperature.

and was expected to cause a significant increase of the diffusion parameter, in agreement with the experimental result.

The focus noise parameter measurements of all the data points of various resists processed under various conditions are summarized in figure 6 right-hand picture. As expected, focus noise is independent of the resist type or process condition. The mean focus noise value is 189 nm, as indicated by the dashed line. The standard deviation is 12 nm. Possible sources that contribute to the observed focus noise are the laser bandwidth combined with the chromatic aberrations of the lens, Z-noise of the wafer stage, and for the scanner, also field curvature.

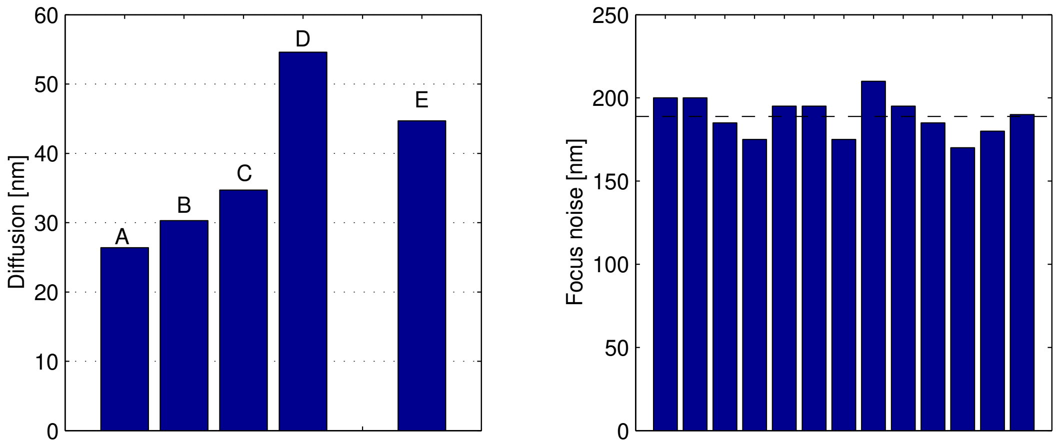

Figure 6. Left: Diffusion parameter σ_r for various resist types. Exposures were made under nominal conditions of PEB time and PEB temperature. The contact hole resist (A) shows the smallest diffusion length. Resist (B) is a a low PEB-sensitive resist. Resist (D) is a modified version of the standard resist (C), containing a smaller PAG. The 157 nm resist (E) is exposed on the $\lambda = 193$ nm scanner. **Right:** A summary of the focus noise parameter for all resists and process conditions. The mean value of 189 nm is indicated by the dashed line.

5. SUMMARY

We have presented a tool, to determine acid diffusion, focus noise and the aberrations of the projection lens from a single experiment. The mathematical framework is the extended Nijboer-Zernike theory, that describes the point-spread function in the presence of diffusion and focus noise. The analysis to retrieve the parameters has been validated by simulations and experiments. The advantage of our approach is a clear separation between the optical parameters like pattern size, illuminator, projection lens aberrations on the one hand and resist parameters on the other.

ACKNOWLEDGMENTS

Philips Research Leuven makes use of the cleanroom facilities of IMEC. The support of the IMEC litho and etch departments, as well as from the IMEC P-Line is greatly appreciated. This work is partly sponsored through the UV2Litho IST-2000-30175 project, and through the Excite MEDEA + T406 project. The authors whish to thank Thomas Steffen from Philips IP&S for the helpfull discussions and carefull reading of the manuscript.

6. APPENDIX

6.1. Normalization of the coordinates

The relationship between normalised image coordinates (x, y), the defocus parameter f and the real space image coordinates (X, Y, Z) in the lateral and axial direction is given by:

$$
\begin{aligned}
x = X\frac{NA}{\lambda} \quad &, \quad y = Y\frac{NA}{\lambda} \\
r = \sqrt{x^2 + y^2} \quad &, \quad (x, y) = (r\cos\phi, r\sin\phi) \\
f \quad &= \quad 2\frac{\pi}{\lambda}Z(1 - \sqrt{1 - NA^2}) \quad ,
\end{aligned}
\tag{7}
$$

with (r, ϕ) polar coordinates in the image plane.

6.2. Definition of the $V_{n,m}$-radial functions

The point-spread function or impulse response of an optical system is the image of an infinitely small object. In practice an object having a diameter of the order of $\frac{\lambda}{2NA}$ is a fair approximation. The Extended Nijboer-Zernike theory is used to calculate the complex amplitude of the aberrated through-focus point-spread function. This calculation involves the radial functions $V_{n,m}(r, f)$. For integers $n, m \geq 0$ with $n - m \geq 0$ and even, the Bessel series representation for $V_{n,m}(r, f)$ reads

$$V_{n,m}(r, f) = \exp(if)\sum_{l=1}^{\infty}(-2if)^{l-1}\sum_{j=0}^{p} v_{lj}\frac{J_{m+l+2j}(v)}{lv^l} \ , \tag{8}$$

with $v = 2\pi r$. The v_{lj} are given by

$$v_{lj} = (-1)^p(m + l + 2j)\binom{m+j+l-1}{l-1}\binom{j+l-1}{l-1}\binom{l-1}{p-j}\Big/\binom{q+l+j}{l}, \tag{9}$$

where $l = 1, 2, \ldots;\ j = 0, \ldots, p$. In Eq. (9) we have set

$$p = \frac{n-m}{2} \quad , \quad q = \frac{n+m}{2}. \tag{10}$$

6.3. Finite hole size

It is favourable to use holes with a non-negligible diameter since the increased amount of light would significantly reduce the required exposure dose, making the experimental procedure much more practical. We assume that the diameter is small compared to the coherence radius of the illumination source, a condition that is almost always fulfilled. The effect of a non-negligible diameter is a drop in amplitude at the rim of the pupil. The extended Nijboer-Zernike theory is sufficiently flexible to account for this effect. The $V_{n,m}(r,f)$ of Eq. (8) should be replaced throughout by

$$\exp(c)V_{n,m}(r, f + id). \tag{11}$$

As one sees from Eq. (8), nothing prevents us from using the Bessel series representation with complex defocus parameter $f + id$. The optimal c, d in Eq. (11) are accurately given as a function of $b = 2\pi a$ by

$$c = \frac{b^4}{2304} + \frac{b^6}{46080}\ ,\ d = \frac{b^2}{8} + \frac{b^4}{384} + \frac{b^6}{10240}\ , \tag{12}$$

with a the normalised diameter of the hole. For details we refer to ref.[12]

6.4. The numerical calculation of the convolution for two radially symmetric functions

Assume we have two radially symmetric functions:

$$g(x,y) = g(\sqrt{x^2+y^2}),\ h(x,y) = h(\sqrt{x^2+y^2}), \tag{13}$$

with g and h fucntions of the radial varaible $r = \sqrt{x^2+y^2} \geq 0$. The 2-D convolution of g and h is radially symmetric as well, and there holds

$$\begin{aligned}(g \otimes h)(x_1, y_1) &= \int\int g(x,y)h(x_1 - x, y_1 - y)dxdy \\ &= \int\int g(\sqrt{x^2+y^2})h(\sqrt{(x_1-x)^2+(y_1-y)^2})dxdy.\end{aligned} \tag{14}$$

It is sufficient to calculate Eq. 14 only for (x_1, y_1) of the form $(r, 0)$; this yields a considerable reduction in CPU- time. As the actual computation of the integral of the right-hand side of 14, it is usuful to note that involved integrands are smooth (unless very small diffusion length are considered) so that the integrals can be discretited without to much problems.

REFERENCES

1. D. Van Steenwinckel, H. Kwinten, S. Locorotondo and S. Beckx, "Overbake: sub-40nm gate patterning with ArF lithography and binary masks" Proc. SPIE 5376 (2004)
2. A.W. Lohmann and D.P. Paris, "Influence of longitudinal vibrations on image quality", Applied Optics, Vol. 4, 1965, p. 393
3. J.Bischoff, W.Henke, J.v.d.Werf, P.Dirksen, "Simulations on step and scan optical lithography", Proc. SPIE 2197 (1994) p. 953
4. D.G. Flagello, J. Mulkens, C Wagner, "Optical lithography into the millennium: Sensitivity to aberration, vibrations and polarization", Proc. SPIE 4000 (2000), p. 172
5. I. Lalovic, A. Kroyan, H. Liu, H. J. Levinson, "Image-blur tolerances for 65 nm and 45 nm-node IC manufacturing", Proc. SPIE 5040 (2003), p. 1570
6. C.N. Ahn, H.B. Kim, K.H. Baik, "A novel approximate model for resist processing", Proc. SPIE 3334 (1998), p. 752
7. D. Fuard, M. Besacier, P. Schiavone,"Assessement of different simplified resist models", Proc. SPIE 4691 (2002), p. 1266
8. D. Fuard, M. Besacier, P. Schiavone, "Validity of the diffused aerial image model: an assessment based on multiple test cases", Proc. SPIE 5040 (2003), p. 1536

9. A.J.E.M. Janssen, "Extended Nijboer-Zernike approach for the computation of optical point-spread functions", *JOSA A* **Vol. 19**, 2002, p. 849
10. J.J.M. Braat, P. Dirksen, A.J.E.M. Janssen, "Assessment of an extended Nijboer-Zernike approach for the computation of optical point-spread functions", *JOSA A* **Vol. 19**, 2002, p. 858
11. P. Dirksen, J. Braat, A. Janssen C. Juffermans, A. Leeuwestein, "Experimental determination of lens aberrations from the intensity point-spread function in the focal region", Proc. SPIE 5040 (2003), p. 1
12. P. Dirksen, J. Braat, A.J.E.M. Janssen, C. Juffermans, "Aberration retrieval using the extended Nijboer-Zernike approach", J. Microlith. Microfab. Microsyst.,**2**, 2003, p. 61
13. W. Hinsberg, F. Houle, M Sanches, J. Hoffnagle, G. Wallraff, D. Medeiros, G. Gallatin, J. Cobb, "Extendibility of chemically amplified resists: another brick wall?", Proc. SPIE Vol. 5039 (2003), p. 1
14. A. Erdmann, W. Henke, S. Robertson, E. Richter, B. Tollkuhn, W. Hoppe, "Comparison of simulation approaches for chemically amplified resists", Proc. SPIE Vol. 4404 (2001), p. 99
15. T. Brunner, R. Ferguson, "Approximate models for resist processing effects", Proc. SPIE 2726 (1996), p. 198
16. SOLID-C, a software product (release 6.3.0) of SIGMA-C GmbH, Thomas-Dehlerstrasze 9, D-81737 Munich, Germany.